Plasmonic enhancement of second harmonic generation from nonlinear $RbTiOPO_4$ crystals by aggregates of silver nanostructures

Laura Sánchez-García,[1,*] Christos Tserkezis,[2,3] Mariola O Ramírez,[1] Pablo Molina,[1] Joan J. Carvajal,[4] Magdalena Aguiló,[4] Francesc Díaz,[4] Javier Aizpurua,[2] and Luisa E. Bausá[1]

[1]*DepartmentoFísica de Materiales and Instituto Nicolás Cabrera, Universidad Autónoma de Madrid, Madrid 28049, Spain*

[2]*Center for Materials Physics (CSIC-UPV/EHU) and Donostia International Physics Center (DIPC), Paseo Manuel Lardizabal 5, Donostia-San Sebastián 20018, Spain*

[3]*Technical University of Denmark, Department of Photonics Engineering, Ørsteds Plads, Building 343, 2800 Kgs. Lynby, Denmark*

[4]*Fisica i Cristal·lografia de Materials i Nanomaterials (FiCMA-FiCNA) and EMaS, Universitat Rovira i Virgili, Tarragona 43005, Spain*

**laura.sanchezgarcia@uam.es*

Abstract: We demonstrate a 60–fold enhancement of the second harmonic generation (SHG) response at the nanoscale in a hybrid metal-dielectric system. By using complex silver nanostructures photochemically deposited on the polar surface of a ferroelectric crystal, we tune the plasmonic resonances from the visible to the near-infrared (NIR) spectral region, matching either the SH or the fundamental frequency. In both cases the SHG signal at the metal-dielectric interface is enhanced, although with substantially different enhancement values: around 5 times when the plasmonic resonance is at the SH frequency or up to 60 times when it matches the fundamental NIR radiation. The results are consistent with the more spatially-extended near-field response of complex metallic nanostructures and can be well explained by taking into account the quadratic character of the SHG process. The work points out the potential of aggregates of silver nanostructures for enhancing optical nonlinearities at the nanoscale and provides an alternative approach for the development of nanometric nonlinear photonic devices in a scalable way.

OCIS codes: (160.2260) Ferroelectrics; (160.4236) Nanomaterials; (160.4330) Nonlinear optical materials; (190.2620) Harmonic generation and mixing; (190.4350) Nonlinear optics at surfaces; (250.5403) Plasmonics.

References and links

1. J. A. Armstrong, N. Bloembergen, J. Ducuing, and P. S. Pershan, "Interactions between light waves in a nonlinear dielectric," Phys. Rev. **127**(6), 1918–1939 (1962).
2. P. Franken, A. E. Hill, C. W. Peters, and G. Weinreich, "Generation of optical harmonics," Phys. Rev. Lett. **7**(4), 118–120 (1961).
3. P. Ferraro, S. Grilli, and P. De Natale, *Ferroelectric Crystals for Photonic Applications*, 2nd ed. (Springer, 2013).
4. B. Chen, M. Ren, R. Liu, C. Zhang, Y. Sheng, B. Ma, and Z. Li, "Simultaneous broadband generation of second and third harmonics from chirped nonlinear photonic crystals," Light Sci. Appl. **3**(7), e189 (2014).
5. A. Arie and N. Voloch, "Periodic, quasi-periodic, and random quadratic nonlinear photonic crystals," Laser Photonics Rev. **4**(3), 355–373 (2010).
6. H. Y. Leng, X. Q. Yu, Y. X. Gong, P. Xu, Z. D. Xie, H. Jin, C. Zhang, and S. N. Zhu, "On-chip steering of entangled photons in nonlinear photonic crystals," Nat. Commun. **2**(8), 429–434 (2011).
7. L. Mateos, P. Molina, J. Galisteo, C. López, L. E. Bausá, and M. O. Ramírez, "Simultaneous generation of second to fifth harmonic conical beams in a two dimensional nonlinear photonic crystal," Opt. Express **20**(28), 29940–29948 (2012).

#259743 Received 19 Feb 2016; revised 4 Apr 2016; accepted 4 Apr 2016; published 11 Apr 2016

8. W. Cai, A. P. Vasudev, and M. L. Brongersma, "Electrically controlled nonlinear generation of light with plasmonics," Science **333**(6050), 1720–1723 (2011).
9. H. Aouani, M. Rahmani, M. Navarro-Cía, and S. A. Maier, "Third-harmonic-upconversion enhancement from a single semiconductor nanoparticle coupled to a plasmonic antenna," Nat. Nanotechnol. **9**(4), 290–294 (2014).
10. N. Kauranen and A. V. Zayats, "Nonlinear plasmonics," Nat. Photonics **6**(11), 737–748 (2012).
11. D. Lehr, J. Reinhold, I. Thiele, H. Hartung, K. Dietrich, C. Menzel, T. Pertsch, E. B. Kley, and A. Tünnermann, "Enhancing second harmonic generation in gold nanoring resonators filled with lithium niobate," Nano Lett. **15**(2), 1025–1030 (2015).
12. E. Yraola, P. Molina, J. L. Plaza, M. O. Ramírez, and L. E. Bausá, "Spontaneous emission and nonlinear response enhancement by silver nanoparticles in a Nd^{3+}-doped periodically poled $LiNbO_3$ laser crystal," Adv. Mater. **25**(6), 910–915 (2013).
13. D. Bar-Lev and J. Scheuer, "Efficient second harmonic generation using nonlinear substrates patterned by nano-antenna arrays," Opt. Express **21**(24), 29165–29178 (2013).
14. L. Sánchez-García, M. O. Ramírez, P. Molina, F. Gallego-Gómez, L. Mateos, E. Yraola, J. J. Carvajal, M. Aguiló, F. Díaz, C. de Las Heras, and L. E. Bausá, "Blue SHG enhancement by silver nanocubes photochemically prepared on a $RbTiOPO_4$ ferroelectric crystal," Adv. Mater. **26**(37), 6447–6453 (2014).
15. M. V. Pack, D. J. Armstrong, and A. V. Smith, "Measurement of the $\chi^{(2)}$ tensors of $KTiOPO_4$, $KTiOAsO_4$, $RbTiOPO_4$, and $RbTiOAsO_4$ crystals," Appl. Opt. **43**(16), 3319–3323 (2004).
16. S. I. Bozhevolnyi, J. M. Hvam, K. Pedersen, F. Laurell, H. Karlsson, T. Skettrup, and M. Belmonte, "Second-harmonic imaging of ferroelectric domain walls," Appl. Phys. Lett. **73**(13), 1814–1816 (1998).
17. J. J. Carvajal, V. Nikolov, R. Solé, J. Gavaldà, J. Massons, M. Aguiló, and F. Díaz, "Crystallization region, crystal growth, and characterization of Rubidium Titanyl Phosphate codoped with Niobium and lanthanide ions," Chem. Mater. **14**(7), 3136–3142 (2002).
18. L. Mateos, L. E. Bausa, and M. O. Ramírez, "Two dimensional ferroelectric domain patterns in Yb^{3+} optically active $LiNbO_3$ fabricated by direct electron beam writing," Appl. Phys. Lett. **102**(4), 042910 (2013).
19. S. V. Kalinin, D. A. Bonnell, T. Alvarez, X. J. Lei, Z. H. Hu, R. J. Shao, and H. Ferris, "Ferroelectric lithography of multicomponent nanostructures," Adv. Mater. **16**(910), 795–799 (2004).
20. E. D. Palik, *Handbook of Optical Constants of Solids* (Academic Press, 2002).
21. Y. Guillien, B. Menaert, J. P. Feve, P. Segonds, J. Douady, B. Boulanger, and O. Pacaud, "Crystal growth and refined Sellmeier equations over the complete transparency range of $RbTiOPO_4$," Opt. Mater. **22**(2), 155–162 (2003).
22. C. L. Mueller, M. A. Arain, G. Ciani, R. T. DeRosa, A. Effler, D. Feldbaum, V. V. Frolov, P. Fulda, J. Gleason, M. Heintze, K. Kawabe, E. J. King, K. Kokeyama, W. Z. Korth, R. M. Martin, A. Mullavey, J. Peold, V. Quetschke, D. H. Reitze, D. B. Tanner, C. Vorvick, L. F. Williams, and G. Mueller, "The advanced LIGO input optics," Rev. Sci. Instrum. **87**(1), 014502 (2016).
23. L. Deyra, X. Délen, G. Mennerat, P. Villeval, F. Balembois, and P. Georges, " Second harmonic generation at 515 nm in RTP with temperature insensitive and non-critical phase matching," in *Advanced Solid-State Lasers Congress*, G. Huber and P. Moulton, eds. OSA Technical Digest (online) (Optical Society of America, 2013), paper AM4A.39.
24. L. K. Cheng, L. T. Cheng, J. Galperin, P. A. M. Hotsenpiller, and J. D. Bierlein, "Crystal growth and characterization of $KTiOPO_4$ and isomorphs from the self-fluxes," J. Cryst. Growth **137**(1–2), 107–115 (1994).
25. F. R. Wagner, A. Hildenbrand, J. Y. Natoli, M. Commandré, F. Théodore, and H. Albrecht, "Laser damage resistance of $RbTiOPO_4$: evidence of polarization dependent anisotropy," Opt. Express **15**(21), 13849–13857 (2007).
26. H. Karlsson, F. Laurell, and L. K. Cheng, "Periodic poling of $RbTiOPO_4$ for quasi-phase matched blue light generation," Appl. Phys. Lett. **74**(11), 1519–1521 (1999).
27. J. N. Hanson, B. J. Rodriguez, R. J. Nemanich, and A. Gruverman, "Fabrication of metallic nanowires on a ferroelectric template via photochemical reaction," Nanotechnology **17**(19), 4946–4949 (2006).
28. E. Yraola, L. Sánchez-García, C. Tserkezis, P. Molina, M. O. Ramírez, J. L. Plaza, J. Aizpurua, and L. E. Bausá, "Controlling solid state gain media by deposition of silver nanoparticles: from thermally- quenched to plasmon-enhanced Nd^{3+} luminescence," Opt. Express **23**(12), 15670–15679 (2015).
29. A. A. Earp and G. B. Smith, "Evolution of plasmonic response in growing silver thin films with pre-percolation non-local conduction and emittance drop," J. Phys. D Appl. Phys. **44**(25), 255102 (2011).
30. A. I. Maaroof and D. S. Sutherland, "Optimum plasmon hybridization at percolation threshold of thin film near metallic surfaces," J. Phys. D Appl. Phys. **43**(40), 405301 (2010).
31. S. A. Maier, *Plasmonics: Fundamentals and Applications* (Springer, 2007).
32. B. Metzger, L. Gui, J. Fuchs, D. Floess, M. Hentschel, and H. Giessen, "Strong enhancement of second harmonic emission by plasmonic resonances at the second harmonic wavelength," Nano Lett. **15**(6), 3917–3922 (2015).

1. Introduction

Nonlinear dielectrics play a key role in modern photonics since they constitute important building blocks in a variety of applications for the efficient control of light. One of the most widely exploited nonlinear phenomena is second harmonic generation (SHG) in which two

#259743 Received 19 Feb 2016; revised 4 Apr 2016; accepted 4 Apr 2016; published 11 Apr 2016

photons of frequency ω are converted into a single photon of frequency 2ω through the creation of a nonlinear polarization. This process is commonly used to convert near-infrared (NIR) radiation into visible light [1,2], usually via the second order susceptibility tensor, $\chi^{(2)}$, of a non-centrosymmetric crystal. Among nonlinear crystals, ferroelectrics have shown a good performance as frequency converters since their symmetry breaking in the ferroelectric phase, together with the possibility of shaping ferroelectric domain structures, allows for a large variety of quadratic nonlinear processes [3–7].

Most of the currently employed frequency-conversion devices are based on birefringent and quasi-phase matching processes. In both cases, the frequency conversion efficiency depends on the device length, and therefore relatively large systems are needed, contrary to the current miniaturization requirements in nanophotonics. An alternative route towards improving the efficiency of frequency conversion phenomena in nanoscale dimensions can be provided by combining nonlinear dielectrics with different materials in hybrid architectures [8–13]. In particular, new light sources can be designed by associating nonlinear dielectrics with metallic nanostructures supporting localized surface plasmon resonances (LSPs) able to strongly confine and enhance the electric fields involved in the nonlinear process. By these means, the inherently weak $\chi^{(2)}$–based frequency conversion phenomena at nanoscale dimensions can take advantage of the extraordinary properties of LSPs to enhance and confine the fundamental electric field at the metal/dielectric interface due to the quadratic character of the nonlinear process on the local fields.

Recently, some of the authors demonstrated the formation of nearly monodisperse Ag nanocubes on the polar surface of the $RbTiOPO_4$ (RTP) ferroelectric crystal by a simple photochemical procedure. The plasmonic modes of the obtained nanocubes were used to enhance the performance of the NIR to visible frequency conversion in the blue spectral region by a factor of around 3 with respect to that obtained from bare RTP [14]. Here we proceed a step further to show that the SHG response of RTP can be enhanced by a factor of around 60 by means of aggregates of silver nanostructures deposited on its polar surface. Specifically, by using different types of Ag nanostructures we show the possibility to tune the plasmonic resonances from the visible to the NIR region to match either the SHG from the RTP crystal in the blue part of the visible spectrum or the NIR fundamental radiation. Consequently, two regimes of enhancement are observed: a low (3-5 times) enhancement obtained when the plasmon resonance shows a maximum at the blue spectral region coinciding with the SHG emission of the nonlinear crystal, and a high enhancement regime (~60 times) achieved when the plasmon resonance matches the fundamental incident radiation in the NIR region. The high intensification factor in the latter case is in agreement with the nonlinear nature of the frequency conversion process, which involves the participation of two fundamental photons to generate a more energetic one with twice the energy.

Additionally, due to the experimental configuration used in our work and to the symmetry of the $\chi^{(2)}$ quadratic susceptibility tensor of RTP [15], the obtained nonlinear response is spatially restricted to the ferroelectric domain boundaries, which, in fact, act as nanosized SHG sources [16], providing additional spatial control on the process. The obtained results are of particular technological relevance since they open the pathway to new efficient frequency-doubling nano-devices in a scalable and cost-effective implementation.

2. Materials and experimental methods

2.1Bulk crystal growth

Ferroelectric RTP single crystals were grown by the top-seeded solution growth (TSSG) method from high temperature. Solutions with a composition Rb_2O-TiO_2-P_2O_5-WO_3 = 42.24-16.80-18.96-20.00 mol% were prepared from Rb_2CO_3, TiO_2, $NH_4H_2PO_4$ and WO_3 precursors in 125 cm^3 cylindrical Pt crucibles. WO_3 was added to the solutions to reduce their viscosity and to facilitate the growth process. A ***c***-oriented crystal seed, located on the surface of the

#259743 Received 19 Feb 2016; revised 4 Apr 2016; accepted 4 Apr 2016; published 11 Apr 2016

solution and on the axis of the Pt crucible, was used for the growth of RTP crystals. The crystal seed was rotated at an angular speed of 45 rpm to favor the homogenization of the solution of growth, and avoid the formation of flux inclusions in the crystals. Further details on the crystal growth procedure can be found elsewhere [17]. For the experiments, 1mm thick plate samples with their main faces perpendicular to the polar axis were cut and polished up to optical grade.

2.2 Domain fabrication

The periodically poled ferroelectric patterns were fabricated by direct electron beam writing by means of a Phillips XL30 Schottky field emission gun electron microscope driven by an Elphy Raith nanolitography software. The electron beam was focused on the ***c***- surface of the RTP crystals. The main experimental parameters used to carry out the inversion process were an acceleration voltage of 15 kV, a beam current of ~450 pA and a charge density of 200 $\mu C/cm^2$. The periodicity of the alternate polar structures studied was 20 μm. The inverted domains were directed along the ***c*** polar axis of the crystal and crossed the whole thickness of the sample (around 1 mm). Details on the procedure can be found elsewhere [18].

2.3 Ag deposition

The photoinduced silver deposition process was carried out by a method previously developed by Kalinin and associates [19]. The polar surface of the ***c***-cut RTP crystals was illuminated with above-bandgap UV light by means of a mercury lamp with its main line at 253.6 nm and emission power of 5400 $\mu W/cm^2$, while the crystal was immersed in a 0.01M $AgNO_3$ solution at room temperature.

2.4 Optical measurements

Extinction spectra were obtained in transmission mode by means of a double beam Lambda 1050 Perkin Elmer spectrophotometer. The extinction spectra of the Ag nanostructures were obtained by subtracting the bare RTP absorption spectrum (which is transparent from 370 to 1000 nm) from those corresponding to the hybrid RTP-Ag nanostructures systems.

Far-field SHG experiments were performed in a laser scanning confocal microscope. A femtosecond Ti:sapphire laser (3900S Tsunami Spectra Physics) tuned at 840 nm was used as a fundamental beam. The laser beam, polarized perpendicular to the domain walls, was focused onto the RTP surface by a 50x microscope objective. The SHG response at 420 nm was collected in backscattering geometry with the same objective and detected by means of a spectrometer and a cooled CCD detector. The samples were placed on a two-axis XY motorized stage in order to register a map of the SHG radiation from the periodically poled RTP crystals. The spatial resolution of the stage was 0.3 μm.

2.5 Numerical simulations

The near-field distribution around the Ag nanostructures, as well as their spectral response, was obtained by solving Maxwell's equations in time domain with perfectly matched layers (PML). A commercial finite-difference-time domain (FDTD) software (Lumerical Solution) was used for the calculations. The computational domain was discretized using grid spacing of 0.5 nm for type A NPs and 0.8 nm for type B. The dielectric function of Ag was obtained by fitting the experimental data from Palik [20]. The refractive index of the RTP substrate was fixed at n = 1.8, according to reference [21].

3. Results and discussion

In this work, periodically poled RTP samples, with their main faces perpendicular to the ferroelectric polar ***c*** axis, were used as nonlinear substrates. RTP is a relevant electro-optic and nonlinear crystal [22,23]. It shows a high ability to grow in large single-domain crystals [24], and a very high optical damage threshold [25]. Furthermore, it shows relatively high

#259743 Received 19 Feb 2016; revised 4 Apr 2016; accepted 4 Apr 2016; published 11 Apr 2016

nonlinear coefficients useful for efficient quadratic frequency conversion in the blue range of the electromagnetic spectrum [26].

The deposition of Ag structures on the RTP polar surfaces was carried out following a low-cost photodeposition procedure by illuminating with UV light the polar surface of the periodically poled RTP samples immersed in an $AgNO_3$ solution at room temperature (see Experimental).

For an illumination time of 2 min, direct formation of silver nanocubes was observed. Figure 1(a) shows a scanning electron microscopy (SEM) image of the resultant nanocubes, which are characterized by an average edge length of around 60 nm and a low size dispersion (around 10%). As previously discussed [14], the well-defined cubic shape and the presence of preferential orientations of the nanocubes suggest the possibility of epitaxial growth related to the crystal structure of the RTP polar surface.

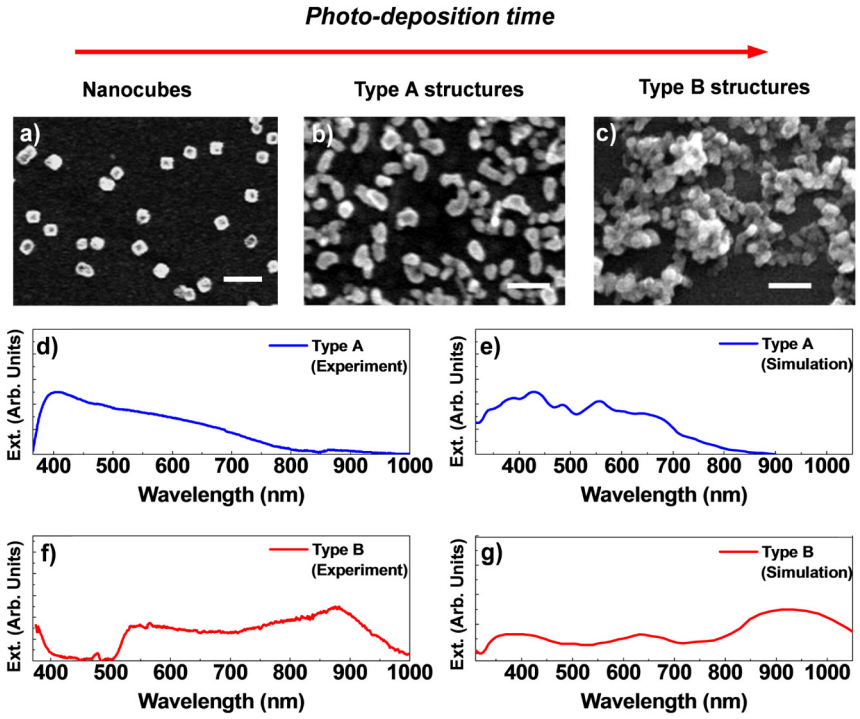

Fig. 1. SEM images of Ag nanostructures obtained on the polar surface of RTP after different photodeposition times. (a) Ag nanocubes (time < 2 min), (b) elongated prism-like shaped Ag nanoparticles (type A structures) (time 4-8 min) and (c) large Ag aggregates (type B structures) (times ≥ 8 min). The scale bars corresponds to 200 nm. (d) Experimental and (e) simulated far field extinction spectra for type A structures. (f) Experimental and (g) simulated far field extinction spectra for type B structures.

Different Ag nanostructures were obtained on the domain surfaces of RTP varying the illumination time. The rest of parameters ($AgNO_3$ concentration, temperature of the substrate, UV flux) were kept constant. Figure 1(b) shows a typical image of the Ag nanostructures obtained for photodeposition times between 4 and 8 minutes. As observed, the deposited structures no longer maintain their cubic shape. Instead, elongated nanoparticles exhibiting nanoprism-shaped structures (hereafter type A structures) are formed. These nanostructures keep the nanocube average width of around ~60 nm and show lengths in the range of 80 - 120 nm.

Finally, for photodeposition times of 8 min and longer, large aggregates of Ag nanoparticles connected in a network-like arrangement with total size of several microns were

#259743 Received 19 Feb 2016; revised 4 Apr 2016; accepted 4 Apr 2016; published 11 Apr 2016

obtained (hereafter type B structures). The corresponding SEM image is displayed in Fig. 1(c).

The different types of metallic nanostructures were obtained separately in different samples by modifying the photo-deposition conditions. In each sample, the plasmonic structures display a uniform morphology all over the surface, as confirmed by scanning electron microscopy images at different areas of the different samples. Additionally, contrary to what has been previously reported for other systems [27,28], no preferential silver deposition (leading to particular aggregates or alignments of nanoparticles) has been observed on the domain boundary surfaces of RTP.

Figures 1(d) and 1(f) show the experimental optical extinction spectra associated with both type A and type B Ag structures, respectively. As expected, they display different plasmonic responses. In particular, type A nanostructures exhibit a broad response covering a good part of the visible spectrum, with the maximum peaking at around 400 nm, and a long decreasing tail down to ~800 nm [Fig. 1(d)]. The more complex type B structures show a quite different plasmonic response,whose main spectral feature is the emergence of a band near 900 nm [Fig. 1(f)] and the decrease of the response at the blue region. Consequently, by varying the silver photodeposition time, it is possible to obtain different metallic arrangements on the polar surface of RTP, thus tuning their plasmonic response from the blue (type A structures) to the NIR region (type B structures). The spectrum of the isolated Ag nanocubes could not be obtained due to the low fractional coverage of these structures on the RTP substrate.

To get better physical insight into the nature of the plasmonic response, detailed FDTD simulations were performed. For type A, the experimental spectrum is well reproduced by considering randomly oriented Ag nanostructures with morphologies and sizes similar to those displayed in Fig. 1(b). Specifically, the representative nanostructures used in our calculations consisted of 60 nm wide nanoprisms with discrete lengths in the range of 80-120 nm. The simulated spectrum is shown in Fig. 1(e). The extinction peak in the blue part of the spectrum is associated with LSP modes corresponding to charge oscillations along the short axis of the nanoprisms, including those related to the Ag-RTP and Ag-air interfaces. On the other hand, the long wavelength extinction tail originates from plasmonic oscillations along the long axis of the nanoprisms. The multiple discrete peaks are due to the relatively few length steps in the simulations, and should disappear for a continuous size and orientation distribution.

The more complex type B Ag structures were modeled as clusters of Ag nanoparticles assembled into a network-like arrangement with a spatial morphology similar to that experimentally observed in Fig. 1(c). The simulated extinction spectrum is displayed in Fig. 1(g). As observed, it qualitatively reproduces the experimental spectral features [Fig. 1(f)], particularly the band around 850-900 nm. It should be noted that the obtained type B structures present certain similarity with systems showing percolation, in which an abrupt step in the electrical and optical properties takes place when metallic isolated nanostructures connect to form large networks. For those systems, the effect of charge delocalization associated with the growth and link of the isolated metallic nanostructures produces a spectral shift of the plasmonic response from the visible region to the near and mid- IR region governed by delocalized plasmons [29,30].

The effect of the obtained metallic structures on the nonlinear properties of RTP is studied by analyzing the blue SHG radiation at 420 nm (around the maximum of the spectral response of type A structures) obtained when the fundamental radiation is set at 840 nm (in the spectral region of type B structures). For the experiments, the fundamental beam is launched along the *c*-axis of the crystal and focused on the surface of the RTP sample. The SHG radiation is collected in backscattering configuration (see Experimental). The sample is set on a two-axis stage, which allows mapping the SHG intensity on the surface of the sample. As previously mentioned, according to the symmetry of the $\chi^{(2)}$ tensor, no SHG should be observed from

#259743 Received 19 Feb 2016; revised 4 Apr 2016; accepted 4 Apr 2016; published 11 Apr 2016

bulk RTP for a fundamental beam propagating parallel to the c-polar direction (z-axis of the nonlinear tensor) [15]. However, the symmetry relaxation at interfaces allows SHG at the ferroelectric domain boundaries, which indeed behave as nanometric nonlinear second harmonic sources [16]. The effect of the different Ag nanostructures on the SHG intensity can be evaluated by comparing the obtained SHG signal before and after the deposition of the Ag structures. Three cases are analyzed: bare RTP, hybrid metal-RTP system with type A silver structures and hybrid metal-RTP system with type B complex aggregates (the effect of the silver nanocubes on the SHG has been the aim of a previous work [14]).

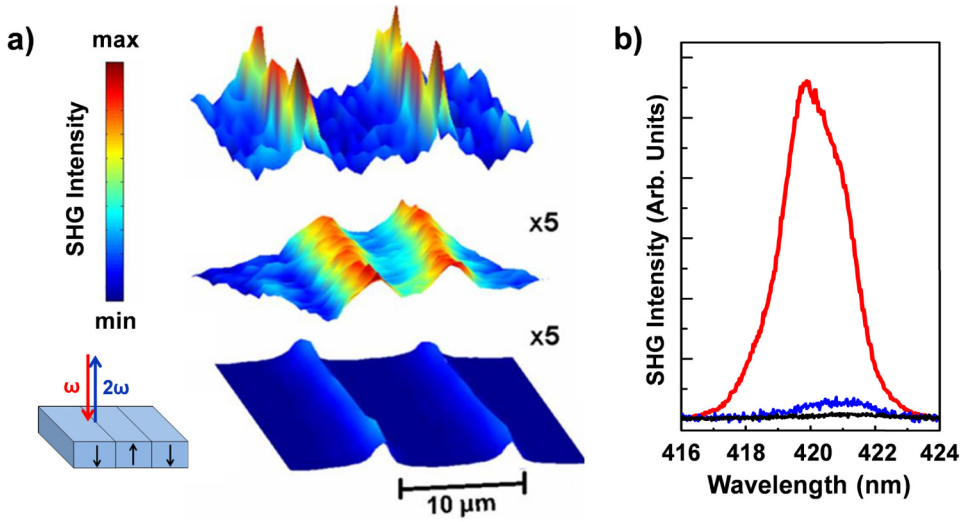

Fig. 2. SHG collected at the domain wall surfaces in backscattering geometry in plasmonic-RTP nonlinear crystals. (a) Schematics of the process and SHG intensity spatial maps of bare periodically poled RTP (bottom), hybrid RTP/type A silver nanostructures (middle) and hybrid RTP/type B complex aggregates (top). For the sake of comparison the SHG intensity corresponding to bare RTP and type A metallic structures have been multiplied by a factor 5. (b) SHG spectra recorded at a single domain wall surface for bare RTP (black), hybrid RTP/type A (blue) and hybrid RTP/type B structures (red).

The spatial maps of the SHG intensity obtained from the RTP surface are depicted in Fig. 2(a). The SHG map at the bottom corresponds to the bare RTP case. As expected, the SHG is produced at the domain boundary surfaces following the ferroelectric domain pattern. After the deposition of metallic nanostructures, the SHG signal becomes more intense and remains localized at the domain walls. This can be seen in the middle and upper maps, which correspond to the SHG response boosted by the presence of type A and type B structures, respectively. Though the silver nanostructures are distributed on the polar surface of RTP, the second harmonic radiation is predominantly generated at the domain walls, so that the contribution of possible nonlinearities associated with the metallic nanostructures can be neglected.

Figure 2(b) shows representative SHG spectra at around 420 nm recorded by focusing the fundamental beam on a single domain wall on the polar surface. The spectrum obtained for bare RTP before Ag deposition (black line) is compared with those obtained when the Ag nanostructures are deposited on the sample. The SHG intensity increases by a factor of around 3 in the presence of type A structures (blue line). On the other hand, in the case of type B complexes (red line) the SHG signal experiences a 60-fold increase.

#259743 Received 19 Feb 2016; revised 4 Apr 2016; accepted 4 Apr 2016; published 11 Apr 2016

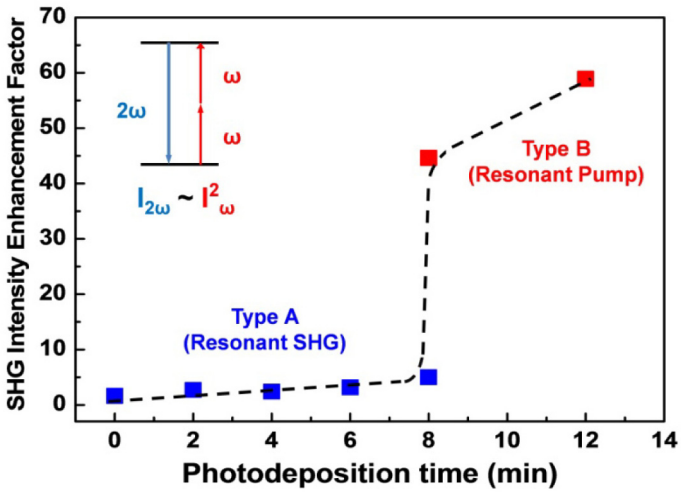

Fig. 3. Experimental SHG intensity enhancement factor as a function of the Ag photodeposition time. The two regimes observed are marked with different colours. The low enhancement regime (blue colour) corresponds to type A nanostructures whose plasmonic response is resonant with the SHG wavelength. The red colour highlights the high enhancement regime, associated with the type B complex aggregates, for which the plasmonic response is resonant with the NIR fundamental radiation. In this case the SHG response is quadratically boosted. The dashed line is a guide for the eye. The inset shows the scheme of levels of the SHG process.

The experimental enhancement factor of the SHG intensity is depicted in Fig. 3 as a function of the Ag photodeposition time, which governs the formation of the different types of Ag structures. The enhancement factor has been defined here as the SHG intensity collected in the presence of Ag structures divided by the intensity obtained from the surfaces of bare RTP. The presence of two different enhancement regimes is clearly revealed by the abrupt step obtained when the photodeposition time increases above 8 min. For shorter times, randomly oriented nanoprisms (type A structures) are formed on the RTP surface and the plasmonic response peaking at the blue range of the spectrum matches well the emitted SHG radiation at 420 nm. This provides a SHG intensification factor in the range of 2 to 5 (blue squares in the figure). For photodeposition times around 8 min and longer, type B Ag structures are formed, with their spectral response matching the fundamental radiation wavelength at 840 nm. In this case, the SHG intensification dramatically increases up to a factor near 60, as depicted by the red squares in Fig. 3.

To analyze the plasmon-enhanced SHG, the near-field distribution around the photodeposited plasmonic nanostructures has been calculated for some representative Ag nanostructures. The results are shown in Fig. 4, where the electric field at the fundamental (840 nm) and SHG wavelength (420 nm) in the proximity of the Ag/RTP interfaces, at 5 nm below the different types of Ag structures, is plotted. To evaluate the plasmon-enhanced SHG response we introduce a phenomenological local field enhancement factor, $g(\omega)$, which accounts for the field enhancement at a frequency ω through $E_{loc}(\omega) = g(\omega)\, E_{inc}(\omega)$, where $E_{loc}(\omega)$ and $E_{inc}(\omega)$ are the local and incident electric field amplitudes, respectively. Therefore, according to the quadratic dependence of the SHG signal on the fundamental radiation, the enhanced SHG intensity, $I(2\omega)$, can be approximated as $I(2\omega) \sim |g(2\omega)|^2\, |g^2(\omega)|^2\, I^2(\omega)$ [31,32], where $I(\omega)$ accounts for the fundamental intensity at the RTP surface without Ag structures.

#259743 Received 19 Feb 2016; revised 4 Apr 2016; accepted 4 Apr 2016; published 11 Apr 2016

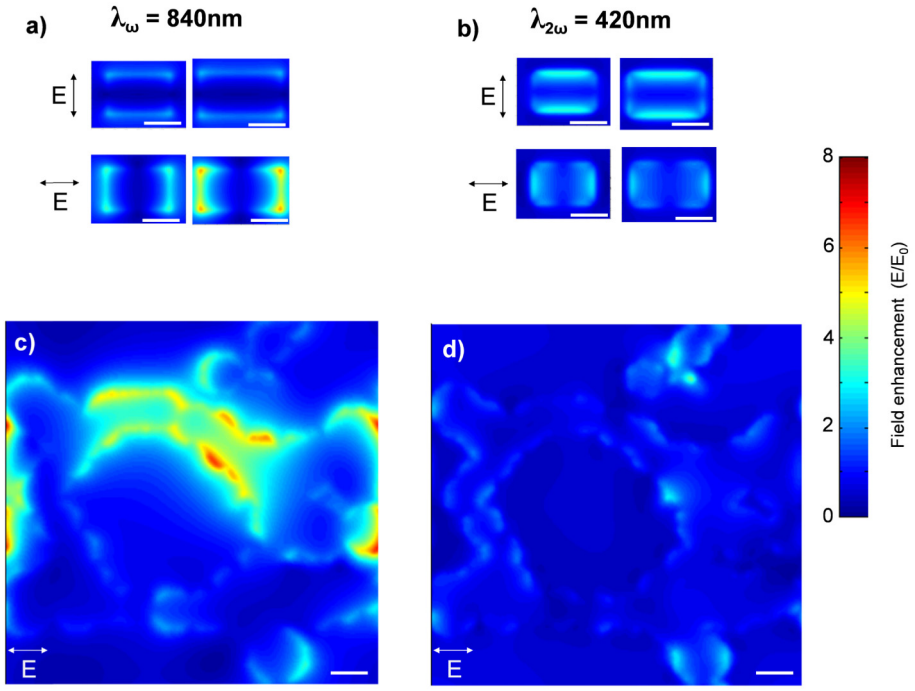

Fig. 4. Calculated near-field intensities for the Ag structures modelled at the fundamental (840 nm) and SH (420 nm) wavelengths 5 nm below the RTP surface. (a) and (b) Electric field enhancement for two representative type A structures corresponding to elongated nanoparticles 80 and 120 nm long (width 60 nm), excited by a plane wave at 840 nm and 420 nm respectively. (c) and (d) Electric field enhancement at the same wavelengths for type B Ag structures. The arrows mark the direction of the incident electric field. In all the panels, the electric field enhancement is depicted with the use of the same colour scale. The scale bar corresponds to 50 nm.

In the case of type A nanostructures, nanoprism-like shaped nanoparticles are distributed with random orientations and a relatively small area coverage on the RTP crystal, producing very small field enhancement at the fundamental frequency. This effect can be easily identified in the near-field distributions displayed in Fig. 4(a), where we show the electric field inside the RTP crystal, at 5 nm below two nanoprisms with different lengths (80 nm, left contours, and 120 nm, right contours), excited at 840 nm by a plane wave polarized along the short or long axis (upper and lower part of Fig. 4(a), respectively). A considerable field enhancement is produced only when long nanoprisms are found on the sample with their long axis parallel to the incident polarization, a situation that occurs only rarely, as observed in Fig. 1(b). This is in agreement with the far-field spectra of Fig. 1(d) where it was shown that the plasmonic response is negligible at the fundamental wavelength (840 nm). On the other hand, at the SH wavelength all the plasmonic type A-nanostructures produce a more spatially-extended near-field enhancement around them and into the RTP crystal [Fig. 4(b)], regardless of their orientation with respect to the polarization of the incident field, thus enhancing the SHG signal mainly through the field enhancement at the SH wavelength. Therefore, in the case of type A structures, $I(2\omega)$, can be approximated by $I(2\omega) \sim |g_A(2\omega)|^2 I^2(\omega)$, $g_A(2\omega)$ being the field enhancement factor of type A structures at the SH wavelength.

In the case of type B structures, a much larger field enhancement is clearly produced at the fundamental frequency [Fig. 4(c)], extending to large areas within the RTP crystal, as expected from the corresponding extinction peak [Fig. 1(f)]. This field enhancement is much less pronounced for the SH wavelength at 420 nm [Fig. 4(d)]. Consequently, for this type of complex Ag aggregates (type B), the contribution from $g_B(\omega)$ dominates the SHG signal

#259743 Received 19 Feb 2016; revised 4 Apr 2016; accepted 4 Apr 2016; published 11 Apr 2016

according to $I(2\omega) \sim |g_B(\omega)|^4 I^2(\omega)$, $g_B(\omega)$ being the field enhancement factor of type B structures at the fundamental wavelength. In this situation, the SHG is enhanced by more than an order of magnitude due to its quadratic dependence on the field enhancement at the fundamental frequency. We can thus conclude that the particular near-field spectral distributions associated with the different morphologies of the plasmonic nanostructures of our two cases, together with the corresponding spatial field extent over a large area below the nanostructures, provide an adequate qualitative and quantitative interpretation of the observed differences in the SHG enhancement. Therefore, despite the complexity of the structures, the tendencies and values derived from the theoretical analysis correlates well with the experimental observations and support the conclusions about the influence of the quadratic dependence of the SHG on the local field enhancement values.

4. Conclusion

In summary, we have shown that by controlling the photodeposition of silver on the polar surface of nonlinear RTP crystals, it is possible to tune the LSP resonances of the Ag structures to match either the fundamental or the SHG radiation wavelength. As a consequence, two enhancement regimes can be achieved: a low enhancement regime (3-5 times), when the plasmon mode is resonant with the blue SHG of the crystal, and a high enhancement regime (60 times) when the plasmon resonance matches the NIR fundamental beam, in agreement with the two-photon character of the SHG process. Furthermore, due to the symmetry of the RTP nonlinear tensor, the blue SHG in our experimental configuration only occurs at the surface of the ferroelectric domain walls. That is, the intensification of the nonlinear response due to the field enhancement of the metallic nanostructures takes place at the nanoscale. The results point out the role of aggregates of silver nanostructures for enhancing SHG processes at metal/dielectric interfaces and open up alternative paths for the development of efficient nanoscale frequency-converter devices in a scalable and low-cost implementation.

Acknowledgments

This work has been supported by the Spanish Ministry of Economy and Competitiveness (MINECO) under projects MAT2013-43301-R, FIS2013-41184-P, MAT2013-47395-C4-4-R and TEC2014-55948-R. The authors also acknowledge Comunidad de Madrid under grant S2013/MIT-2740, Dept. of Industry of the Basque Country under project nanoGUNE'14, and Catalan Authority under project 2014SGF1358. F.D. acknowledges additional support through the ICREA Academia awards 2010ICREA-02 for excellence in research. LSG acknowledges FPU13/02476 grant from the Spanish Ministry of Education.

#259743 Received 19 Feb 2016; revised 4 Apr 2016; accepted 4 Apr 2016; published 11 Apr 2016